Fermi surface study of $LaRu_2Si_2$ and of heavy-fermion $CeRu_2Si_2$ above the Kondo temperature

M. A. Monge,* M. Biasini,† G. Ferro,‡ and M. Gemmi
ENEA, Via Don Fiammelli 2, 40128 Bologna, Italy

G. Satta and S. Massidda
Istituto Nazionale di Fisica della Materia (INFM) and Dipartimento di Fisica Università degli Studi di Cagliari, 09124 Cagliari, Italy

P. Lejay
CRTBT, Avenue de Martyrs, Boîte Postale 166, 38042 Grenoble Cedex 9, France

A. Continenza
Istituto Nazionale di Fisica della Materia (INFM) and Dipartimento di Fisica, Università degli Studi dell'Aquila, I-67010 Coppito (L'Aquila), Italy

(Received 4 April 2001; revised manuscript received 13 July 2001; published 3 January 2002)

The Two-dimensional (2D) angular correlation of the positron annihilation radiation of the heavy-fermion system $CeRu_2Si_2$ was measured above the Kondo temperature T_K and compared to that of the reference isostructural non-f-electron system $LaRu_2Si_2$. The $\boldsymbol{k}$-space densities of the two compounds, obtained via the Lock-Crisp-West folding of the 3D-reconstructed electron-positron momentum densities, were very similar. These results are in reasonable agreement with the band structure calculated for $CeRu_2Si_2$ using the local-density approximation (LDA). Conversely, in the case of $LaRu_2Si_2$, a clear discrepancy between the LDA calculation and the experiment appears unless the Fermi level (E_F) is raised by ~ 11 mRy. After the E_F adjustment the calculated Fermi surfaces are rather similar and in agreement with both experiments. The implications of this similarity on the physics of the heavy fermions are discussed.

DOI: 10.1103/PhysRevB.65.035114 PACS number(s): 71.18.+y, 75.10.Lp, 78.70.Bj

I. INTRODUCTION

The heavy-fermion (HF) compound $CeRu_2Si_2$ is often considered the archetype system displaying the *standard heavy-fermion behavior*.[1,2] With an electronic specific-heat coefficient $\gamma = 350$ mJ/K^2 mole (≈ 300 times higher than the γ of simple metals, such as Mg or Cr), it shows neither magnetic ordering nor superconductivity down to temperatures of few mK. Indeed, the magnetic susceptibility deviates from the Curie-Weiss behavior at temperatures T lower than the Kondo temperature T_K ($T_K \sim 20$ K in $CeRu_2Si_2$) approaching a temperature dependence typical of Pauli paramagnets.[3] The magnetic moment obtained from the high-temperature region of the magnetic susceptibility curve ($\mu_{eff} = 2.64\mu_B$ for magnetic field perpendicular to the c axis[4]) is close to the value obtained applying Hund's rules to Ce^{3+} atom ($\mu_{eff} = 2.53\mu_B$) and consistent with a localized $4f$ electron description. On the other hand, the existence of a paramagnetic ground state was explained assuming that the hybridization and consequent formation of the Kondo singlets between $4f$ electrons and conduction electrons produces narrow bands (with dispersion $\Delta \approx k_B T_K$) responsible of a high density of states at E_F and accounting for the γ value and the cyclotron masses observed at $T \ll T_K$.[5,6] At $T \geqslant T_K$, the temperature excitations should cause the $4f$ electrons to decouple from the conduction (s,p,d) electrons and not to contribute to the Fermi surface (FS). Therefore, according to this conjecture,[1,2] the Fermi volume at $T > T_K$ should decrease by one electron, resembling that of the isostructural non-f-electron compound $LaRu_2Si_2$.

The de Haas–van Alphen (dHvA) experiments,[5,6] performed at temperatures much lower than T_K, seem to indicate that in $CeRu_2Si_2$ the $4f$ states do contribute to the FS. This is suggested by a reasonable agreement between the FS calculated within the local-density approximation (LDA) to density functional theory, where the $4f$ electrons are treated as ordinary band electrons (i.e., itinerant), and the measured one.[5–7] Moreover, the dHvA experiments claim a change in the $4f$ electron character across the metamagnetic transition at the critical field $B_m \sim 7.7$ T. In the high-field region some low-field dHvA frequencies are replaced by others, similar to those observed for $LaRu_2Si_2$, and some cyclotron masses decrease dramatically.[8,9] Although the underlying mechanism is not fully understood, the properties of the transition bear some resemblance with those of a magnetic ordering to be ascribed to the $4f$ electrons. This would suggest that in the magnetically ordered state the $4f$ electrons decouple from the conduction electrons. Conversely, neutron diffraction experiments[10] and measurements of the static magnetization[11] indicate that the itinerant character of the $4f$ electrons is unaffected by the metamagnetic transition.

These controversial findings suggest to pursue the investigation of this compound. In particular, the study of the electronic structure in the high-temperature regime with suitable experimental techniques is essential to test the applicability of the ''so-called'' *standard heavy-fermion behavior* that, in brief, implies itineracy of the f electrons at $T \ll T_K$ and localization at higher temperatures.[12] The test of the

Fermi volume at $T>T_K$ is precluded to the dHvA experiments, due to the shortening of the electron mean free path in the cyclotron orbits with increasing temperature. The two-dimensional angular correlation of the position annililation radiation (2D-ACAR) experiment, which is not restricted to very low temperatures, appears to be a valid tool to elucidate the issue.

This experiment, by measuring the distribution $N(\theta_x,\theta_y)$ of the deviation angles from anticollinearity of the annihilation γ rays, determines a 2D projection of the 3D electron-positron (ep) momentum density $\rho^{ep}(\boldsymbol{p})$,[13] which can be expressed (in atomic units) as

$$\rho^{ep}(\boldsymbol{p})=\sum_{n,\boldsymbol{k}}^{occ}\left|\int \exp(-i\boldsymbol{p}\cdot\boldsymbol{r})\,\psi_{\boldsymbol{k}}^{n}(\boldsymbol{r})\,\phi(\boldsymbol{r})\,g(\boldsymbol{r})\,d\boldsymbol{r}\right|^2. \quad (1.1)$$

Here $\psi_{\boldsymbol{k}}^{n}$ and ϕ denote the one-particle electron and positron wave function, respectively, and the summation extends over all occupied electron states with Bloch wave vector $\boldsymbol{k}$ from energy bands of index n. The factor $g(\boldsymbol{r})$ accounts for the ep correlations.[14,15] In periodic systems, $\rho^{ep}(\boldsymbol{p})$ is discontinuous at points $\boldsymbol{p}_{F_l}=(\boldsymbol{k}_{F_l}+\boldsymbol{G})$, where $\boldsymbol{G}$ is a reciprocal lattice vector and $\boldsymbol{k}_{F_l}$ are the reduced Fermi wave vectors in the first Brillouin zone (BZ). The standard Lock-Crisp-West (LCW) transformation,[16] extensively used in the data analysis of the 2D-ACAR spectra, reinforces these discontinuities by folding the momentum distribution $\rho^{ep}(\boldsymbol{p})$ back onto the first BZ by translation over the appropriate vectors $\boldsymbol{G}$. If the summation is performed over a sufficient portion of momentum space the result, denoted here as $\rho_{LCW}^{ep}(\boldsymbol{k})$, is[17]

$$\rho_{LCW}^{ep}(\boldsymbol{k})=\sum_{n}\ \theta(E_F-\epsilon_{k,n})\int |\psi_k^n(\boldsymbol{r})|^2|\phi(\boldsymbol{r})|^2 g(\boldsymbol{r})\,d\boldsymbol{r}. \quad (1.2)$$

Here $\epsilon_{k,n}$ is the energy eigenvalue of the electron $\boldsymbol{k}$ from band n. In general, although the mapping of the FS is facilitated when the overlap integral in Eq. (1.2) is a weakly varying function of $\boldsymbol{k}$, the FS discontinuities [marked by the step function of Eq. (1.2)] are not shifted by this $\boldsymbol{k}$ dependence.[18] In practice, to obtain the 3D image of the FS, it is necessary to reconstruct the 3D $\rho^{ep}(\boldsymbol{p})$ from its 2D projections using tomographic techniques and then perform the 3D LCW folding.

Positron annihilation experiments on the heavy fermion $CeCu_2Si_2$ (Ref. 19) indicated that even at $T>T_K$ an *f*-electron itinerant calculation (f band) was in better agreement with the experiment than an *f*-electron localized calculation (f core). However, in that case only a small part of the FS had been mapped by dHvA and found to agree mostly with the *f*-core calculation.[20]

In this work we report a comprehensive analysis of our 2D-ACAR experiments on $CeRu_2Si_2$ and the isostructural reference non-*f*-electron system $LaRu_2Si_2$. The measurements are complemented by *ab initio* band-structure calculations obtained via the full potential linearized augmented plane wave (FLAPW) method[21] within the LDA. The comparison between theory and experiments is performed including the effects of the nonuniform positron density and of the ep correlations [as described by Eqs. (1.1) and (1.2)]. The results on $CeRu_2Si_2$ seem to indicate (unexpectedly) that a standard LDA calculation (implying a zero temperature) can account for the electronic structure observed above T_K. However, the close similarity between the spectra of the two compounds and the results of the LDA calculations lead to the conclusion that one is unable, on the base of LDA, to give an univocal answer about the itineracy of the *f* electrons in $CeRu_2Si_2$ at any temperature.

II. EXPERIMENTAL PROCEDURES AND DETAILS OF THE CALCULATIONS

The crystal structures of $CeRu_2Si_2$ and $LaRu_2Si_2$ are body centred tetragonal (BCT), containing one molecule per primitive cell. The space group is $I4/mmm$.

The single crystals were prepared by direct combination of high purity starting materials [Ce, La, and Ru $4N$, Si $6N$], for a total weight of nearly 10 g. The raw elements were melted in a water-cooled copper crucible heated with a high-frequency generator under a purified argon atmosphere. The melt was then introduced in a tri-arc furnace under inert gas, equipped with a Czochralski puller.[22] The single crystals were grown from the bulk starting composition using single crystalline seeds. An x-ray diffraction experiment, using the von Laue technique in back reflection, confirmed the final single crystalline state. Moreover, samples were annealed in a resistive ultrahigh vacuum furnace during eight days at 950 °C under a vacuum of 3.5×10^{-10} torr. The lattice constants, refined using a Rietveld procedure from the powder, were $a=4.197(2)$ Å, $c=9.801(4)$ Å and $a=4.217(5)$ Å, $c=9.938(4)$ Å, for $CeRu_2Si_2$ and $LaRu_2Si_2$, respectively.

The 2D-ACAR experiments were carried out with a new setup based on a pair of Anger cameras and described in detail in Ref. 23. The estimated overall experimental resolution was (0.08,0.13) a.u. for the p_x and p_y directions of the spectrometer, corresponding to 12% and 20% of the shortest size of the BZ ($4\pi/c$), respectively.

Data were accumulated in a (288×288) matrix with a bin size of (0.02×0.02) a.u.^{2}, at the temperature of ≈60 K in a vacuum of $\sim1\times10^{-6}$ torr. The 3D $\rho^{ep}(\boldsymbol{p})$ was reconstructed rotating the crystal about the fourfold [001] axis, which was normal to the integration directions. The five projections collected for both materials, each amounting to $\approx3\times10^8$ raw coincidence counts, spanned uniformly the angle comprised between the [100] and the [110] axes. Moreover, to monitor temperature differences due to a change in the character of the *f* electrons, the [100] projection for $CeRu_2Si_2$ was also collected at room temperature. The spectra were corrected for the distortions due to the finite angular field of view and the spatial variations in the single detector efficiencies.[24] Finally, the van Citter–Gerhardt deconvolution alghorithm was applied.[25] This method combines the simplicity of the van Citter[26] iterative procedure with the ability of not enhancing the noise. The reconstruction was performed (on planes perpendicular to the main symmetry axis, $\boldsymbol{p}_x\equiv[001]$) according to the Cormack's method[27] and to a modification of the filtered-back-

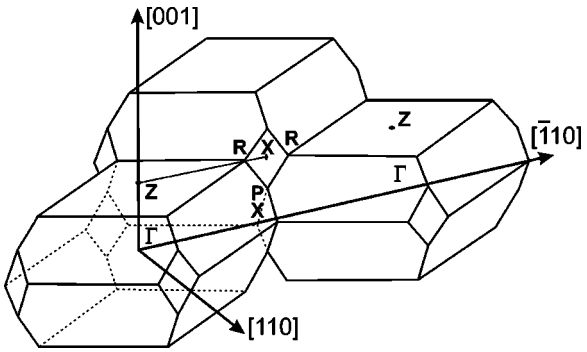

FIG. 1. BZ of the BCT $CeRu_2Si_2$ and $LaRu_2Si_2$ in a repeated zone scheme. The labeling describes the BZ high symmetry points.

projection method described elsewhere.[28,29] Both algorithms exploit the crystal symmetry and can provide a faithful reconstruction of $\rho^{ep}(\boldsymbol{p})$ from a small number of projections, depending on the amount of its anisotropy. In this case five projections proved to be adequate. Finally, the 3D-LCW transformation was applied.[16] Since the main features of the $\boldsymbol{k}$-space density $\rho^{ep}_{LCW}(\boldsymbol{k})$ provided by two reconstruction methods were rather similar, only the Cormack's results will be shown next.

Calculations of $\rho^{ep}(\boldsymbol{p})$ were carried out using the self-consistent FLAPW method[21] within the LDA. The experimental lattice parameters reported above were adopted. In the interstitial region, the plane waves expansion was truncated at the maximum wave vector $K_{max}=3.3$ a.u. Inside the muffin-tin spheres, we used spherical harmonics with angular momenta up to $l_{max}=6$ for the potential and charge density, and up to $l_{max}=8$ for the wave functions. The muffin tin radii were $R_{Ce}=3$ a.u., $R_{Ru}=2.4$ a.u., and $R_{Si}=2.1$ a.u. The calculation of the K states was performed within the exact BZ of the BCT structure (shown in Fig. 1). For the self-consistency iterations we used 300 independent k points and the linear tetrahedra method. To fine tune the Fermi level value and to determine the band occupancy over the BZ we performed a spline fit of the energy bands (in terms of a Fourier series over direct lattice vectors), and then we calculated the fitted bands over a 128^3 mesh points in the BZ. The numerical accuracy of our Fermi level is estimated to be of the order of 1 mRy. The momentum density was calculated on a 10^3 mesh in the BZ.

Further information was gained by an LDA calculation (denoted as f core) that treated the $4f$ electron of $CeRu_2Si_2$ as core states. This was accomplished by forcing a Ce $4f^1$ core configuration. The energy parameter for the $4f$ orbitals was set at very high value (~ 2 Ry) thus excluding the Ce f component from the valence states.

The potential adopted for the positron wave function calculation was obtained by summing to the inverted crystal Coulomb potential a term due to the electron-positron correlations, within an LDA scheme suggested by Boronski and Nieminen.[14] The electron-positron annihilation enhancement, $g(\boldsymbol{r})$, was also included. The contribution of core levels, expected to be rather small, was neglected.

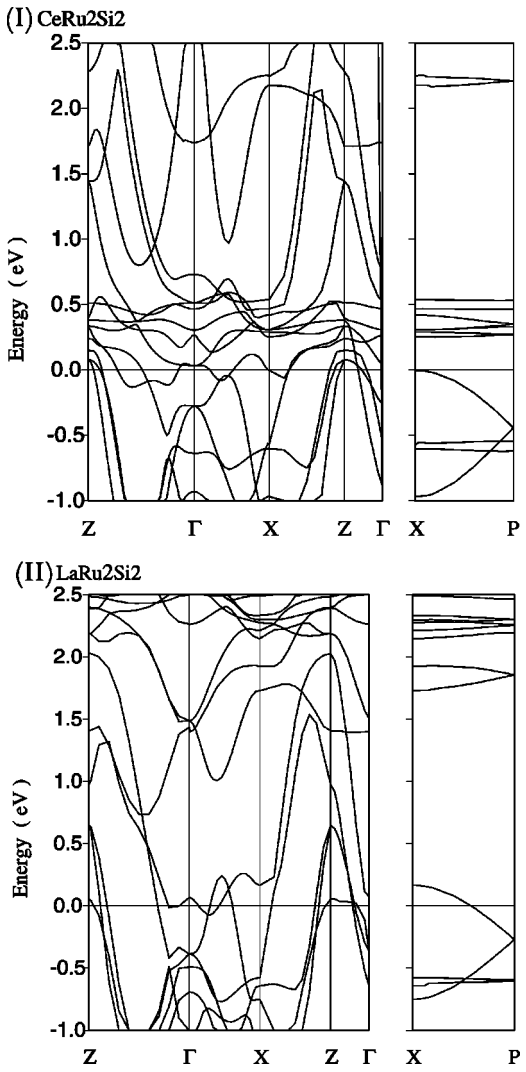

FIG. 2. I. Energy bands of $CeRu_2Si_2$ calculated with a self-consistent FLAPW calculation along high symmetry directions of the BZ. All the energies are referred to the Fermi level, set to zero. II. Same as I for $LaRu_2Si_2$.

III. RESULTS AND DISCUSSIONS

We start our discussion by showing in Fig. 2 the energy bands for $CeRu_2Si_2$ (including f electrons in the valence bands) and $LaRu_2Si_2$, respectively. Figure 2I shows that in $CeRu_2Si_2$ the flat $4f$ bands lie mostly above E_F. Nevertheless, they contribute significantly (by about 50% within LDA) to the high value of the density of states at E_F. The energy bands for $LaRu_2Si_2$ (Fig. 2II) are very similar to those of $CeRu_2Si_2$. We can see important differences only near E_F. For both materials, the bands and the resulting five FS sheets are in good agreement with those reported in Ref. 7.

Figure 3 shows the positron density along high symmetry planes of the unit cell for $CeRu_2Si_2$. A very similar picture (not shown) results in the case of $LaRu_2Si_2$. It appears that the positron is sampling the unit cell rather uniformly, apart from the nuclear regions where it is strongly repelled by the positive ionic charge. Therefore, it is expected that all the

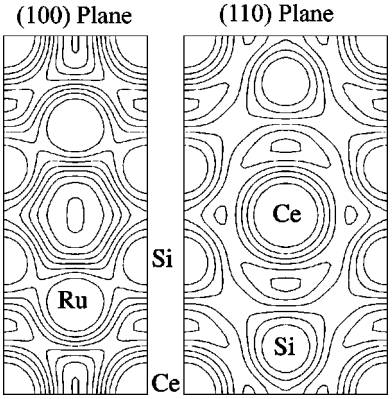

FIG. 3. Contour plots of the positron density in $CeRu_2Si_2$, on the (100) and (110) planes of the unit cell cutting the Ce atoms at the origin of coordinates. The spacing between contour levels is 10^{-3} e/a.u.^{3}, and the positron density at the nuclear positions is zero.

conduction bands will contribute with significant discontinuities to ρ^{ep}_{LCW}.

This prediction is to some extent confirmed by the reasonable amplitude variation of the 3D experimental $\rho^{ep}_{LCW}(\boldsymbol{k})$ densities for both materials, notwithstanding the low crystal symmetry, the small sizes of the BZ and the numerous fully occupied bands. Indeed, the total amplitude variations of $\rho^{ep}_{LCW}(\boldsymbol{k})$ were 6.2% and 8.2% of their maxima for $CeRu_2Si_2$ and $LaRu_2Si_2$, respectively. Figure 4I(a) shows one slice of $\rho^{ep}_{LCW}(\boldsymbol{k})$ for $CeRu_2Si_2$ at $k_z=0$ in a repeated zone scheme. The most evident pattern consists of high-intensity regions centered at the X symmetry points of the BZ. These structures, in the following denoted by η, are visible in any slice of $\rho^{ep}_{LCW}(\boldsymbol{k})$ normal to the [001] direction.

Moreover, two concentric low-intensity regions centred at the Z points appear. The inner region, marked by the white arrow in Fig. 4I(a) and in the following denoted by β, has a roughly prolate ellipsoidal shape with full width at half maximum (FWHM) $\approx$0.16 a.u. in the $k_z=0$ plane and FWHM $\approx$0.19 a.u. along the [001] direction. Its cross-sectional area through the $k_z=0$ plane corresponds to a dHvA frequency $F_{dHvA}\approx 9\times 10^6$ G. This value is approximately averaging the experimental F_{dHvA} for magnetic field parallel to [001], denoted by β_1 and β_2 in references,[5,6] and the corresponding hole-FS sections (of very similar sizes) calculated by us and others[7] for $LaRu_2Si_2$ and $CeRu_2Si_2$. The related energy bands have mostly Ru d-like character in $LaRu_2Si_2$ and admixture of Ce f-like and Ru d-like character in $CeRu_2Si_2$. Nevertheless, the topology predicted by LDA for these FS sheets is very similar in the two compounds.

To compare appropriately our FLAPW calculation with the 2D-ACAR experiments we calculated $\rho^{ep}(\boldsymbol{p})$, according to Eq. (1.1), over the finite field of view of the experiment [$\sim(2\times 2.56$ a.u.$)^3$] and applied the LCW folding. The result, for the $k_z=0$ plane, is shown in Fig. 4I(b). In Figs. 4I(c) and 4I(d) the same procedure was applied after shifting the Fermi level of 5 mRy upward and downward, respectively. The low-intensity region centered at the Z points of the theoretical panels of Fig. 4I is consistent with the four

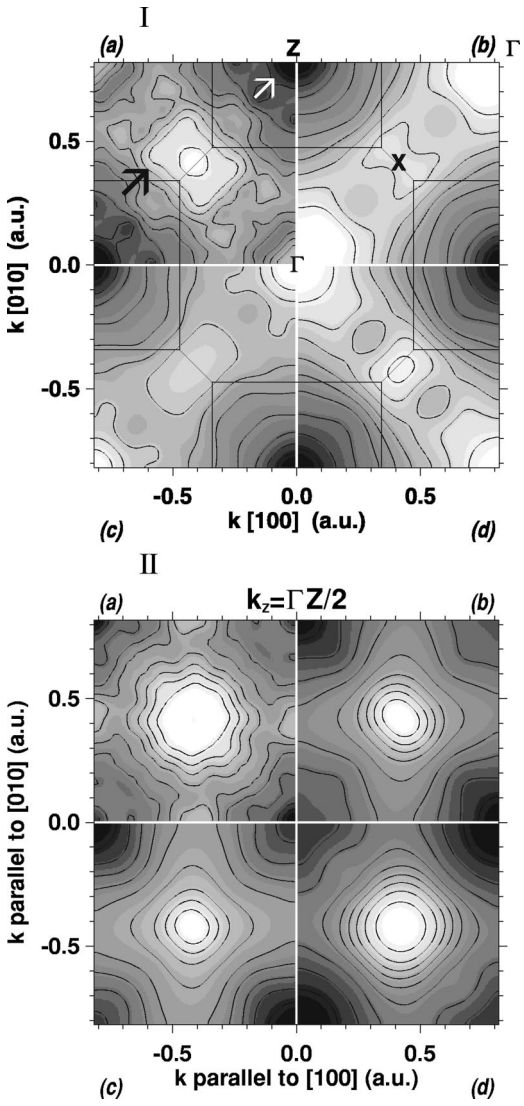

FIG. 4. I. Experimental and calculated k-space densities for $CeRu_2Si_2$ in a repeated zone scheme for the plane $k_z=0$. The intersection of the BZs with the $k_z=0$ plane is shown. (a) Experimental $\rho^{ep}_{LCW}(\boldsymbol{k})$. The black arrow indicates the contour surrounding the η structures discussed in the text. The white arrow indicates the β structure (see text). The contour level spacing corresponds to 0.6% of the maximum. (b) $\rho^{ep}_{LCW}(\boldsymbol{k})$ obtained by LCW folding the theoretical $\rho^{ep}(\boldsymbol{p})$ calculated over the finite experimental field of view. (c) Same as (b) after shifting E_F downward of 5 mRy. (d) Same as (b) after shifting E_F upward of 5 mRy. II. Same as Fig. I for the plane $k_z=\overline{|\Gamma Z|}/2$. In this and all following gray scale figures white corresponds to high intensity and black to low intensity. The labeling indicates the high symmetry points of the BZ. 1 a.u.$=1/a_0$ $=1.89$ Å^{-1}, where a_0 is the Bohr radius. The matrix sizes are equivalent to $(4\pi/a)\times(4\pi/a)$.

Z-centered holelike FS's. Moreover, the sparse high-intensity zone surrounding X and Γ (denoting the theoretical counterpart of the experimental η structure) reflects the occupancy of the uppermost (fifth) conduction band. The Z-centered low-intensity regions are in fair agreement with the experiment [shown in Fig. 4I(a)]; conversely, the calculated η structures are much more extended than the experimental

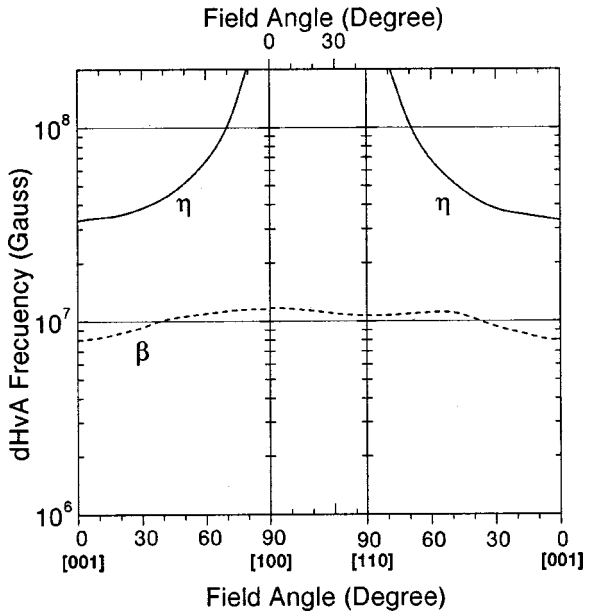

FIG. 5. Angular dependence of the dHvA frequencies pertaining to the η and β FS sheets observed in this work for $CeRu_2Si_2$.

ones. The agreement between experiment and theory improves noticeably in other planes of the BZ. Fig. 4II shows the same comparisons as figure 4I for a plane equidistant from Γ and Z. The columnar structures centered at $\sim(0.4,0.4)$ a.u. appear clearly in experiment and theory and the low-intensity regions at the center and at the $\sim(0,0.8)$ a.u.-type points are in reasonable agreement as well. The shift in the Fermi level of 5 mRy below or above E_F has the effect to shrink or swell the η columnar structures, respectively, but does not change substantially the general features of the resulting $\rho^{ep}_{LCW}(\boldsymbol{k})$. In Fig. 4I(a) the black arrow selects a contour at the half maximum of the η structure. The corresponding F_{dHvA}, $F_{dHvA}=3.4\times10^7$ G, was observed in $CeRu_2Si_2$ (Refs. 5–7) and not in $LaRu_2Si_2$. The angular dependence of the extremal cross-sectional areas (transformed into F_{dHvA} frequencies) for isodensities corresponding to the η and the β sheets discussed above is shown in Fig. 5. The functional angular dependence turns out to be rather insensitive to the values of $\rho^{ep}_{LCW}(k)$ selected (once and for all) for the isocontour sections. The angular dependence for the β sheet is in good agreement with the dHvA experiments.[5,6] The η sheet was observed by dHvA only in a small angular range nearby the (001) plane.[5–7] However, Fig. 7 of Ref. 7, predicts nonclosed orbits in the [001] direction, consistent with Figs. 4(a) and 5.

Figures 6(a) and 6(b) show a 3D view of the isodensity surface selected at the half maximum of the η experimental structures [highlighting the $\boldsymbol{k}$ loci of the largest amplitude variation of $\rho^{ep}_{LCW}(\boldsymbol{k})$] and the calculated electronlike FS sheet due to the uppermost conduction band for $CeRu_2Si_2$ (the calculated holelike FS's resulting from the other four conduction bands, very similar to those of Ref. 7, are not shown). It appears that the η structures observed in the experiment [Fig. 6(a)] are limited to the columnar part of the calculated multiply connected electron FS [Fig. 6(b)]. The results of the *f-core* calculation relative to the uppermost conduction bands are shown in Fig. 6(c). It appears that the extent of the experimental high intensity) η structures and low intensity Z-centered regions are in better agreement with

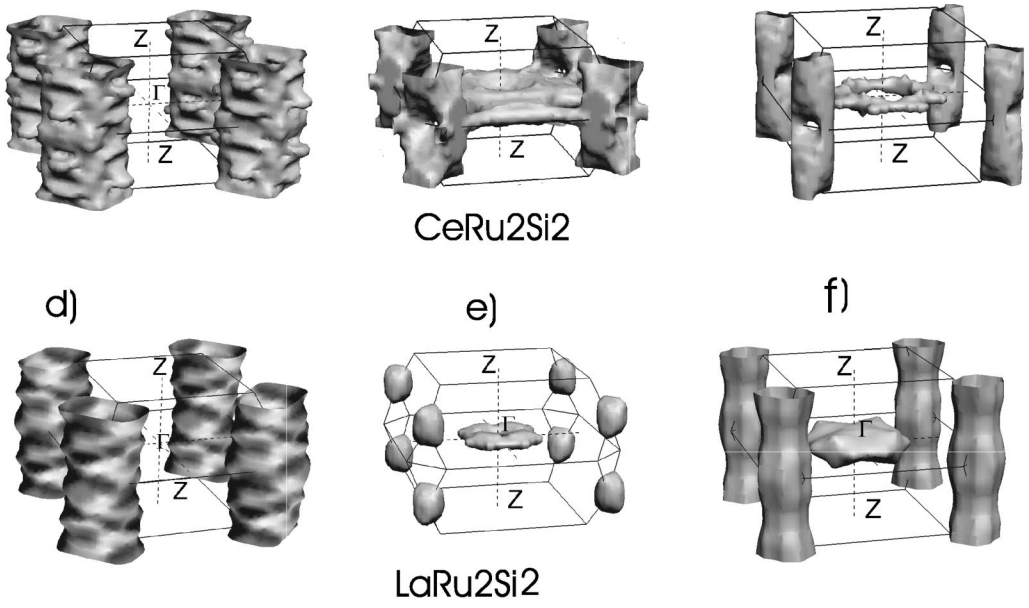

FIG. 6. (a) 3D view of the experimental η structures for $CeRu_2Si_2$ (see text). (b) FS sheet pertaining to the uppermost conduction band in $CeRu_2Si_2$ calculated according to the *f*-band model (see text). To facilitate the FS visualization, the top and bottom part of the Fermi volume (few percent of $4\pi/c$) are not shown. The labeling indicates the high symmetry points of the BZ. (c) FS sheet pertaining to the uppermost conduction band in $CeRu_2Si_2$ calculated according to the *f*-core model (see text). (d) 3D view of the experimental η_L columnar structures described in the text in the case of $LaRu_2Si_2$. (e) Same as (b) for $LaRu_2Si_2$. (f) Calculated FS sheet pertaining to the uppermost conduction band in $LaRu_2Si_2$ after shifting E_F upward of 11 mRy (see text).

TABLE I. Fermi volumes in percent of BZ of the experimental FS's and the five FS sheets resulting from the FLAPW theory. For $CeRu_2Si_2$ the results of the *f*-band and *f*-core calculations (see main text) are reported. For $LaRu_2Si_2$, values obtained after the shift in E_F of $+11$ mRy are also shown. The experimental FS's were identified as the isodensity surfaces taken at the value of the half-maximum of the structures in question (see text).

	$CeRu_2Si_2$			$LaRu_2Si_2$		
FS sheet (band $n°$)	Expt	Theory *f* band	Theory *f* core	Expt	Theory ($\Delta E_F=0.$)	Theory ($\Delta E_F=+11$ mRy)
Electron (15)	18 ± 5	19.1	3.7	13 ± 4	1.2	11
Hole (14)	20 ± 8	14.9	41.7	21 ± 5	48.7	35
Hole (13)		3.3	5.6		3.3	2.1
Hole (12)	0.7 ± 0.5	1.3	3.1		1.3	0.5
Hole (11)		0.3	0.3		0.1	0.05

the *f*-band calculation. On the other hand, the low intensity of the experimental $\rho^{ep}_{LCW}(\boldsymbol{k})$ in the (001) plane nearby the Γ point [shown in Fig. 6(a)] is in better agreement with the corresponding intensity of the calculated $\rho^{ep}_{LCW}(\boldsymbol{k})$ according to the *f*-core model.

Since the temperature of our measurements ($T\sim60$ K) was rather close to T_K ($T_K\sim20-30$ K), the two 2D-LCW spectra of the projection along the [100] direction for $CeRu_2Si_2$, collected at room temperature and at 60 K (see Sec. II), were inspected for possible differences. The analysis showed that, apart from the modest degradation in the experimental resolution due to the positron motion ($\sim20\%$), no temperature effect attributable to a change in the character of the *f* electrons was observed.

Since the agreement between experiment and either calculation (*f* band, *f* core) was not complete we thought it appropriate to complement the measurements on $CeRu_2Si_2$ with those of the isostructural non-*f*-electron system $LaRu_2Si_2$. In this case, according to LDA, the flat bands having high $4f$ electron character are ~2.5 eV above E_F (see Fig. 2II). Therefore, this measurement should clarify uncertainties concerning the contribution of the *f* electrons to the Fermi volume in $CeRu_2Si_2$.

The main differences between the FLAPW calculations for the two compounds are due to the fact that whereas $CeRu_2Si_2$ is a compensated metal, with equal volumes enclosed by electronlike and holelike FS's, $LaRu_2Si_2$ has one hole carrier per formula unit. Consequently, the large multiply connected electron FS sheet calculated for $CeRu_2Si_2$ shrinks, in $LaRu_2Si_2$, into eight small disconnected ellipsoids [see Figs. 6(b) and 6(e)]. Moreover, the holelike FS due to the 4th conduction band swells considerably. A surprise of the calculation was that the Fermi volume of the uppermost band of $LaRu_2Si_2$ (corresponding to 1.2% of the BZ volume) is about three times smaller than what obtained for the equivalent band by the *f*-core calculation in $CeRu_2Si_2$ [compare Fig. 6(e) with Fig. 6(c)]. We attribute this difference to the critical shapes of the conduction bands in these systems. This example shows that conclusions on the character of the *f* electrons drawn on the base of calculations of the isostructural non-*f*-electron systems may be incorrect. Nevertheless, the full comparison between the Fermi volumes yielded by the calculations, listed in Table I, shows that the *f*-core calculation for $CeRu_2Si_2$ and the standard LDA calculation for $LaRu_2Si_2$ give rather similar results.

A much greater surprise was provided by the measurement of $LaRu_2Si_2$, which revealed columnar patterns in the [001] directions, having very similar shape to the η struc-

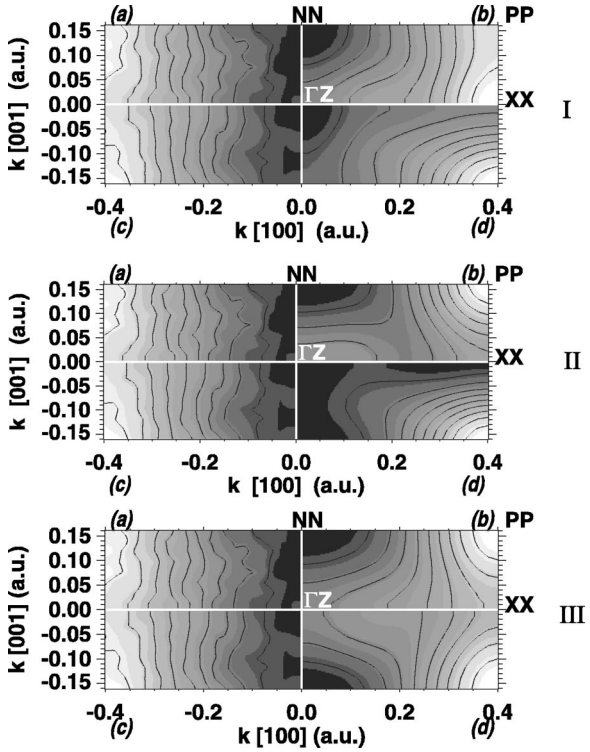

FIG. 7. Quadrants (a) and (c) always refer to the 2D $\rho^{ep}_{LCW}(\boldsymbol{k})$ densities obtained from the experimental projections along the [010] axis for $CeRu_2Si_2$ and $LaRu_2Si_2$, respectively. The contour level spacing corresponds to 0.3% of the maximum, equivalent to seven times the statistical uncertainty of the maximum. The various calculations reported in quadrants (b) and (d) result from the integration of the 3D theory along the [010] direction and its convolution with the asymmetric experimental resolution. I(b) Theoretical $\boldsymbol{k}$-space density (occupancy) for $CeRu_2Si_2$. (d) same as (b) for $LaRu_2Si_2$. II(b) Calculated $\rho^{ep}_{LCW}(\boldsymbol{k})$ for $CeRu_2Si_2$. (d) same as (b) for $LaRu_2Si_2$. III(b) $\rho^{ep}_{LCW}(\boldsymbol{k})$ obtained by LCW folding the $\rho^{ep}(\boldsymbol{p})$ calculated over the finite experimental field of view. (d) the same as (b) for $LaRu_2Si_2$ but here E_F was shifted upward of 11 mRy. The labeling describes the projected BZ high symmetry points. The matrix sizes are equivalent to $(2\pi/a)\times(2\pi/c)$.

TABLE II. Wave-function orbital character of $CeRu_2Si_2$ inside the Ce spheres for two $\boldsymbol{k}$ points located on the Γ plane [$\boldsymbol{k}_1 \simeq (\pi/2a, \pi/2a, 0)$] and inside the η structures [$\boldsymbol{k}_2 \simeq (\pi/a, \pi/a, \pi/c)$]. Bands 14 and 15 refer to the two uppermost conduction bands. The last column denotes the energy eigenvalue referred to the Fermi level, E_F.

State	(band $n°$)	s	p	d	f	E-E_F (mRy)
$\boldsymbol{k}_1$	14	0.000 00	0.019 67	0.121 04	0.152 00	−7.3
$\boldsymbol{k}_1$	15	0.000 00	0.004 32	0.147 62	0.180 30	−1.0
$\boldsymbol{k}_1$	16	0.000 00	0.001 92	0.008 63	0.734 86	+9.1
$\boldsymbol{k}_2$	14	0.000 00	0.001 55	0.010 80	0.027 73	−36.9
$\boldsymbol{k}_2$	15	0.000 00	0.043 30	0.069 94	0.088 77	−19.9
$\boldsymbol{k}_2$	16	0.000 00	0.000 01	0.000 27	0.963 27	+16.0

tures of $CeRu_2Si_2$. Figure 6(d) shows an isodensity surface selected at the half maximum of these columns (in the following denoted by η_L). Their full width at half maximum in the ZXZ direction (FWHM≈0.26 a.u.) is only slightly smaller (∼9%) than the corresponding width for $CeRu_2Si_2$. On the purely experimental point of view, the similarity between Fig. 6(a) and Fig. 6(d) would indicate that the f electrons do not play a major role in the determination of the Fermi volume, unlike what suggested by the reasonable agreement between experiment and LDA f-band calculation. Nevertheless, the clear discrepancy between experiment and calculation in $LaRu_2Si_2$ [compare Fig. 6(d) and Fig. 6(e)] demands a study of the stability of the experimental results.

To prove that this discrepancy is neither related to positron wave-function effects nor due to an insufficient experimental resolution, nor to artifacts due to the reconstruction procedure, we compared *raw projected data* to the calculation suitably processed. To this end, Fig. 7 refers to *projections* along the [010] direction, which is particularly suitable to appraise the extent of the η and η_L columns. Therefore, we show next the 2D-LCW folded data of the 2D-ACAR measurements. The remarkable similarity of the 2D spectra of $CeRu_2Si_2$ and $LaRu_2Si_2$ [shown in quarters (a) and (c) of Fig. 7, respectively] along the XX-PP direction confirms the existence of the columnar structures, η and η_L, shown in Figs. 6(a) and 6(d). Although the experimental spectra were subjected to our deconvolution procedure, the projections of the various calculations [shown in quarters (b) and (d) for $CeRu_2Si_2$ and $LaRu_2Si_2$, respectively] were convoluted with the asymmetric experimental resolution. The additional smearing was meant to assess whether a slight overestimation of the resolution could prevent to observe the interruption of the electron cigars along the [001] direction shown in Fig. 6(e). Figures 7I(b) and 7I(d) show the projected electron occupancies, confirming the features present in Figs. 6(b) and 6(e): for $CeRu_2Si_2$, the high intensity of the occupancy along the XX-PP directions is consistent with the experiment [quadrant (a)]. However, unlike the experimental case, the contour lines show a protrusion toward the ΓZ point [consistent with Fig. 6(b)]. The most interesting result concerns $LaRu_2Si_2$ [Fig. 7I(d)]: even an overestimated experimental resolution is not smearing sufficiently the high-intensity regions centred at the PP corners, in clear discrepancy with the experiment.

The effect of the nonuniform positron density is taken into account in Figs. 7II(b) and 7II(d), showing the projected $\rho^{ep}_{LCW}(\boldsymbol{k})$. It can be noticed that in Fig. 7II(b) the intensity of $\rho^{ep}_{LCW}(\boldsymbol{k})$ along the XX-ΓZ direction is lower than the electron occupancy [Fig. 7II(a)] in the same direction.

These results can be better understood by looking at the orbital character (s,p,d,f) of the wave functions of two representative $\boldsymbol{k}$ points, belonging to the Γ plane ($\boldsymbol{k}_1$) or to the η columns ($\boldsymbol{k}_2$), respectively. Table II reports the characters of $\boldsymbol{k}_1$ and $\boldsymbol{k}_2$ inside the sphere of the Ce atom for bands 14th up to 16th (where 14 and 15 denote the two uppermost conduction bands). Since the contribution of the f orbitals in $\boldsymbol{k}_1$ of bands 14 and 15 is higher than in $\boldsymbol{k}_2$, the localization of $\boldsymbol{k}_1$ increases at the expenses of the ep matrix elements and, consequently, of $\rho^{ep}_{LCW}(\boldsymbol{k})$ in the Γ plane. In fact, as the positron resides prevalently in the interstices (see Fig. 3), annihilations with electron states characterized by a large interstitial character of the wave function are favored at the expenses of states more localized, i.e., more confined nearby the ionic centres (typically unhybridized d like or $f$like). Concerning $LaRu_2Si_2$, Fig. 7II(d) shows no substantial change with respect to Fig. 7I(d) (electronic occupancy) along the PP-XX direction.

Figs. 7III(b) and 7III(d) were obtained by applying the 2D-LCW transformation to a projection of the calculated $\rho^{ep}(\boldsymbol{p})$ which included only the finite field of view of the spectrometer.

The two-dimensional analysis of the LDA f-core calculation for $CeRu_2Si_2$ (not reported here) shows structures centred at the PP points, rather similar to those produced by the standard LDA calculation for $LaRu_2Si_2$, which are inconsistent with either experiment.

Moreover, Fig. 7III(d), showing a much better agreement beween experiment and calculation [compare Fig. 7III(c) and Fig. 7III(d)], was obtained by shifting the Fermi level upward of 11 mRy (∼0.15 eV). The main effect of the shift is to fill $\boldsymbol{k}$ states of the uppermost conduction band nearby the $k_z=0$ and $k_z=\overline{|\Gamma Z|}$ plane, causing the small cigars shown in Fig. 6(e) to swell and connect in the [001] direction (see the energy bands of Fig. 2II along the direction XP). A 3D view of the FS sheet produced by the uppermost band after the 11 mRy shift of E_F in $LaRu_2Si_2$ is shown in Fig. 6(f).

It is somewhat surprising that such a modest shift, within the order of the adjustments often operated to bring theory and dHvA experiment into closer agreement,[30] produces such

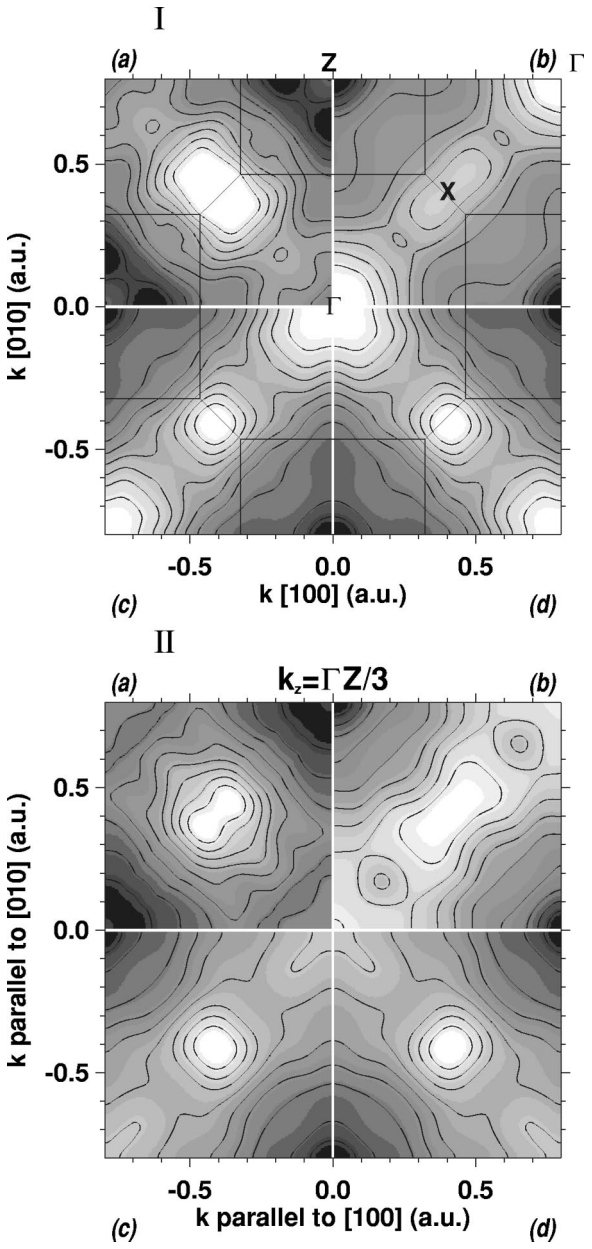

FIG. 8. I. Experimental and calculated *k*-space densities for $LaRu_2Si_2$ in a repeated zone scheme for the plane $k_z=0$. (a) Experimental $\rho^{ep}_{LCW}(\boldsymbol{k})$. The contour level spacing corresponds to 0.8% of the maximum. (b) $\rho^{ep}_{LCW}(\boldsymbol{k})$ obtained by LCW folding the calculated $\rho^{ep}(\boldsymbol{p})$ limited to the experimental field of view. (c) and (d) Same as (b) after shifting E_F upward of 11 mRy. II. Same as Fig. I in the plane $k_z=\overline{|\Gamma Z|}/3$. The labeling indicates the high symmetry points of the BZ. The matrix sizes are equivalent to $(4\pi/a)\times(4\pi/a)$.

a remarkable effect. While this shift is somehow arbitrary, we should remember that there is no guarantee that LDA eigenvalues reproduce correctly the quasiparticle excitations of the system. For example, it is well known that in semiconductors LDA yields a large error in the band gap (self-energy correction), sometimes giving a semimetallic band structure for small gap insulators. The electronic properties of ordinary metals are usually better reproduced by LDA. Nevertheless, states with different orbital character may need different self-energy corrections, leading to modifications of the LDA band structure (see Ref. 31 for the limiting case of oxides). This is certainly the case of *d*-derived bands nearby E_F such as those produced by the Ru (but also La and Ce) *d* states in $LaRu_2Si_2$ and $CeRu_2Si_2$.

Figure 8 shows slices of the 3D-reconstructed experimental (quadrants *a*) and calculated (quadrants *b*,*c*,*d*) $\rho^{ep}_{LCW}(\boldsymbol{k})$ density in the $k_z=0$ (part I) and $k_z=\overline{|\Gamma Z|}/3$ (part II) planes for $LaRu_2Si_2$. As for Fig. 4, we calculated $\rho^{ep}(\boldsymbol{p})$ over the finite field of view of the experiment and applied the LCW folding. Whereas quadrant (b) refers to the unchanged FLAPW calculation, quadrants (c) or (d) were obtained shifting E_F upward of 11 mRy. As for Fig. 7III(d), after the energy shift the columnar structures appear at any section of the BZ normal to the [001] axis, in agreement with the experiment.

A summary of the Fermi volumes obtained from experiments and calculations is shown in Table I. The theoretical values were obtained from the occupancies of each conduction band. The experimental values were yielded by the volumes included by isodensity surfaces selected at the half maxima of the structures discussed above. It can be noted that the small closed surface denoted as β in $CeRu_2Si_2$ could not be resolved in $LaRu_2Si_2$, possibly because of its small sizes. Owing to the numerous bands contributing to the FS and the modest experimental resolution, the experimental uncertainty is rather high. Nevertheless, we note a reasonable agreement between experiment and *f*-band calculation for $CeRu_2Si_2$. Conversely, in the case of $LaRu_2Si_2$ the discrepancy is much larger, of one order of magnitude for the uppermost conduction-band Fermi volume and of a factor 2 for the fourth-band Fermi volume. It should be noted that owing to the large extent of the η_L experimental structure in the [001] direction, a holelike FS centred at *Z* cannot possibly occupy the volume predicted by the theory. After the shift of E_F the discrepancy between theory and experiment is softened at the expense of an incorrect total Fermi volume (expected to correspond to one electron per formula unit).

We completed our analysis by testing the effect of shifting the Fermi level upward of 11 mRy in the case of $CeRu_2Si_2$ as well. We should point out that the operation of shifting the Fermi level (which is linked to the correct number of electrons per cell) should actually be replaced by shifts of the bands relative to each other, in such a way as to simulate the (unknown) self-energy corrections of the different electron states. Bearing this in mind, we can briefly summarize the results (not shown here) as follows.

(1) As is the case of $LaRu_2Si_2$ the occupancy of the uppermost (electronlike) conduction band increases and that of the lower (holelike) conduction bands decrease noticeably. The resulting occupancy is strongly deviating from the experimental one.

(2) These large discrepancies with the experiments are somewhat reduced after the insertion of the electron-positron matrix elements that, as discussed at length in the two-dimensional analysis, are smaller in the Γ plane than along the *XP* directions. We surmise that this positron wavefunction effect reduces the sensitivity of the experiment to

subtle changes in the electronic structure.

Recently,[32] we have proposed a method to estimate the density of states at the Fermi energy, $N(E_F)$, and, consequently, the electronic specific-heat coefficient γ from the 2D-ACAR data. $N(E_F)$ is defined as

$$N(E_F)=\frac{1}{4\pi^3}\int_S \frac{dS}{|\nabla_k \epsilon|}, \tag{3.1}$$

where the integral is over the FS and $\gamma=N(E_F)\pi^2 k_B^2/3$. As Eq. (3.1) shows, $N(E_F)$ depends on the FS, experimentally available, and on the gradient of the energy function at $\boldsymbol{k}_F$, $\nabla_k \epsilon$, which is inaccessible to the 2D-ACAR experiment. One could adopt for $|\nabla_k \epsilon|$: (i) the free electron model expression ($|\nabla_k \epsilon|=\hbar^2 k_F/m$), (ii) the average gradient at $\epsilon(k_F)$ obtained from a band-structure calculation.

Both approaches are inapplicable to heavy fermions, owing to the well-known inability of standard LDA to reproduce the γ values. Therefore, we limit ourselves to $LaRu_2Si_2$, adopting the average energy gradients calculated by our FLAPW method. The calculation yields an overall density of states at the Fermi level E_F (before the shift in E_F discussed above), $N(E_F)=42$ States/(Ry cell), corresponding to $\gamma_{calc}\simeq 7.1$ mJ/(mole K^2).

From the experiment, the FS sheet attributed to the η_L structures [Fig. 6(d)] yields $\gamma=(2.9\pm 0.6)$ mJ/(mole K^2) and $N(E_F)=(17\pm 4)$ States/(Ry cell) (using $|\nabla_k \epsilon|=2.7$ eV/a.u.), whereas for the hole like structure centred at Z (see Table I) we obtain $\gamma=(3.7\pm 1.)$ mJ/(mole K^2) and $N(E_F)=(22\pm 7)$ States/(Ry cell) (using $|\nabla_k \epsilon|=3.7$ eV/a.u.). The overall γ value [$\gamma_{expt}=(6.6\pm 1.2)$ mJ/(mole K^2)] is remarkably close to the experimental value obtained with the traditional calorimetric measurements [$\gamma=6.5$ mJ/(mole K^2)].[33] Owing to the uncertainties in the extent of the FS determined experimentally and in the appropriate values of $|\nabla_k \epsilon|$ such a close agreement is probably fortuitous. Nevertheless, it is worth emphasizing that although the experimental FS differs from the theoretical one (prior to the E_F shift), it is not incompatible with the most relevant thermodynamic measurements.

One may wonder whether the existence of the η and η_L structures can be suggested by other measurements. A rather indirect evidence was provided by the measurements of the magnetoresistance in $CeRu_2Si_2$ and $LaRu_2Si_2$ by Onuki *et al.*[5] By investigating the angular dependence of the magnetoresistance in $CeRu_2Si_2$ the authors inferred the existence of open electron orbits along the c axis, consistent with our measurements. The absence of an angular dependence of the magnetoresistance in $LaRu_2Si_2$ led the authors to the conclusion that no open orbit could be present in that system. However, no dHvA frequencies which could be attributed to close orbits in the cigars shown in Fig. 6(e) were detected in $LaRu_2Si_2$.[5]

IV. CONCLUSIONS

Up to now, much of our understanding of the heavy fermion behavior was based on the archetype compound $CeRu_2Si_2$ where, unlike other heavy fermion systems, an FS based on an electron itinerant description seemed to yield a better agreement with the experiments. Our results at $T>T_K$, complemented by the measurements on $LaRu_2Si_2$, suggest a different interpretation.

(1) The similarity of the two experimental spectra ($LaRu_2Si_2$, $CeRu_2Si_2$) supports the nonitineracy of the f electrons in $CeRu_2Si_2$ at $T>T_K$. This result may not seem surprising, as it confirms the standard heavy fermion behavior conjectures. However, the distinction of our results appears by comparing the experiments to the (state of the art) LDA calculations.

(2) The FS similarities attained by the calculations [compare figures 6(b), 6(c), 6(f)] after the modest aforementioned shift in the Fermi energy suggest that the agreement between an f electron itinerant description and previous experiments (at $T\ll T_K$) in $CeRu_2Si_2$ may be coincidental. Indeed, the Ru d part of the LDA bands produces most of the features which characterize the FS of both materials. Owing to these *pathological* features of the bands, LDA seems to be unable to elucidate the issue at stake.

The unexpected results obtained here by comparing the 2D-ACAR experiments on $CeRu_2Si_2$ and $LaRu_2Si_2$ suggest to complement the early 2D-ACAR measurements at $T>T_K$ on $CeCu_2Si_2$,[19] which supported an f-band calculation, with a corresponding investigation of the $LaCu_2Si_2$ system.

An unsatisfactory result of our findings for $LaRu_2Si_2$ is that the Fermi volume obtained by experiment and theory (after the shift in the Fermi energy) is inconsistent with what expected for a noncompensated metal.

Finally, one must take into account the previous dHvA measurements on $LaRu_2Si_2$ that claim differences with respect to the $CeRu_2Si_2$ case, in support of an f-electron itinerant description in $CeRu_2Si_2$. However, no dHvA frequency consistent with the FS sheet predicted by LDA for the uppermost conduction band of $LaRu_2Si_2$ [small electron cigars shown in Fig. 6(e)] was ever observed. The dHvA frequencies consistent with the small holelike FS (three lowest conduction bands) are almost the same as those seen in $CeRu_2Si_2$. Therefore, the whole belief in the *standard heavy-fermion behavior* is based in the observation of only one frequency (denoted as α in Refs. 5 and 7), ascribed to the FS sheet of the fourth band calculated by LDA for $LaRu_2Si_2$ and never observed in $CeRu_2Si_2$. Taking into account that dHvA experiments cannot locate the extremal FS cross sections in the BZ and in the light of our proposed measurements, we believe that the *standard heavy-fermion behavior* description is based on insufficient premises. At this stage, it not clear whether the concepts of itineracy and localization utilised in the standard LDA limit are appropriate to describe heavy fermions. In this regard, among the realistic (*ab initio*) band-structure calculations recently implemented, the self-interaction correction, known to increase the localization of the one-electron spatial wave functions,[34,35] the "LDA+U" method, which aims at accounting for the strong on-site atomiclike correlation effects of the $4f$ electrons,[36] or the dynamic field theory, which adopts the single impurity Anderson model imbedded in an effective medium determined self consistently,[37] could be employed to describe ap-

propriately a small hybridisation of the $4f$ electrons with the conduction electrons.

Within the LDA limit, only the discovery of a $4f$ itinerant HF system with an FS radically different from that of a comparable $4f$ localized system could elucidate the puzzle of the f electron character in heavy fermions.

ACKNOWLEDGMENTS

We thank B. Luethi and G. Kontrym-Sznajd for their contribution to this work, and A. Mauri for help with instrumentation.

*Permanent address: Dpto. Física, Universidad Carlos III, Av. Universidad 30, 28911 Leganés (Madrid), Spain.

†Also at Istituto Nazionale di Fisica della Materia Corso Perone 24, 16152 Genova, Italy.

‡Corresponding author. Email address: Biasini@bologna.enea.it

[1] P. Fulde and G. Zwicknagl, Physica B **206-207**, 125 (1995); G. Zwicknagl, Phys. Scr. T **49**, 34 (1993).

[2] F. Steglich, C. Geibel, K. Gloos, G. Olesch, C. Schank, C. Wassilew, A. Loidl, A. Krimmel, and G.R. Steward, J. Low Temp. Phys. **95**, 3 (1994).

[3] In this regard, it is worth recalling that recent muon spin rotation (μ^+SR) experiment at $T<2$ K have unveiled the existence of very low static magnetic moments ($\mu_s \simeq 0.001 \mu_B$/Ce), questioning the paramagnetic character of the ground state. See A. Amato, Rev. Mod. Phys. **69**, 1119 (1997), and references therein.

[4] P. Haen, J. Flouquet, F. Lappiere, P. Lejay, and G. Remenyi, J. Low Temp. Phys. **67**, 287 (1987).

[5] Y. Onuki, I. Umehara, A.K. Albessard, T. Ebihara, and K. Satoh, J. Phys. Soc. Jpn. **61**, 960 (1991).

[6] F.S. Tautz, S.R. Julian, G.J. McMullan, and G.G. Lonzarich, Physica B **206-207**, 29 (1995).

[7] H. Yamagami and A. Hasegawa, J. Phys. Soc. Jpn. **61**, 2388 (1992); **62**, 592 (1993).

[8] H. Aoki, S. Uji, A.K. Albessard, and Y. Onuki, Phys. Rev. Lett. **71**, 2110 (1993).

[9] H.P. van der Meulen, A. de Visser, J.J.M. Franse, T.T.J. Berendschot, J.A.A.J. Perenboom, H. van Kempen, A. Lacerda, P. Lejay, and J. Flouquet, Phys. Rev. B **44**, 814 (1991).

[10] J.L. Jacoud, L.P. Regnault, J. Rossat-Mignod, C. Vettier, P. Lejay, and J. Floquet, Physica B **156&157**, 818 (1989).

[11] T. Sakakibara, T. Tayama, K. Matsuhira, H. Mitamura, H. Amitsuka, K. Maezawa, and Y. Onuki, Phys. Rev. B **51**, 12 030 (1995).

[12] Some authors denote the critical temperature for the change of nature of the *f* electrons as *coherence* temperature (Ref. 1) but its definition was never fully clarified.

[13] S. Berko, *Positron Solid-State Physics*, edited by W. Brandt and A. Dupasquier (North Holland, Amsterdam, 1983), p. 64.

[14] E. Boronski and R.M. Nieminen, Phys. Rev. B **34**, 3820 (1986).

[15] A. Rubaszek, Z. Szotek, and W.M. Temmermann, Phys. Rev. B **58**, 11 285 (1998).

[16] D.G. Lock, V.H. Crisp, and R.N. West, J. Phys. F: Met. Phys. **3**, 561 (1973).

[17] J.H. Kaiser, R.N. West, and N. Shiotani, J. Phys. F: Met. Phys. **16**, 1307 (1986).

[18] C.K. Majumdar, Phys. Rev. A **140**, 227 (1965).

[19] D. Vasumathi, B. Barbiellini, A.A. Manuel, L. Hoffmann, T. Jarlborg, R. Modler, C. Geibel, F. Steglich, and M. Peter, Phys. Rev. B **55**, 11 714 (1997).

[20] M. Hunt, P. Meeson, P.A. Probst, P. Reinders, M. Springford, W. Assmus, and W. Sun, J. Phys.: Condens. Matter **2**, 6859 (1992).

[21] H.J.F. Jansen, and A.J. Freeman, Phys. Rev. B **30**, 561 (1984); M. Weinert, H. Krakauer, E. Wimmer, and A.J. Freeman, *ibid.* **24**, 864 (1981).

[22] P. Lejay, J. Muller, and R. Argoud, J. Cryst. Growth **130**, 238 (1993).

[23] M. Biasini, G. Ferro, M. Monge, G. di Francia, and V. La Ferrara, J. Phys.: Condens. Matter **12**, 5961 (2000).

[24] R.N. West, J. Mayers, and P.A. Walters, J. Phys. E **14**, 478 (1981).

[25] U. Gerhardt, S. Marquardt, N. Schroeder, and S. Weiss, Phys. Rev. B **58**, 6877 (1998), and references therein.

[26] P.H. van Citter, Z. Phys. **69**, 298 (1931).

[27] A.M. Cormack, J. Appl. Phys. **35**, 2908 (1964).

[28] G. Kontrym-Sznajd and E. Jozefczuk, Mater. Sci. Forum **255-257**, 754 (1997), and references therein.

[29] M. Biasini, M.A. Monge, G. Kontrym-Sznajd, M. Gemmi, and N. Sato, Mater. Sci. Forum **363-365**, 582 (2001).

[30] Among the many examples, see C.A. King and G.G. Lonzarich, Physica B **171**, 161 (1991), where this procedure was adopted to the isostructural compound $CeRu_2Ge_2$.

[31] See, for example, S. Massidda, R. Resta, M. Posternak, and A. Baldereschi, Phys. Rev. B **52**, R16 977 (1995); S. Massidda, A. Continenza, M. Posternak, and A. Baldereschi, *ibid.* **55**, 13 494 (1997).

[32] M. Biasini, G. Kontrym-Sznajd, M.A. Monge, M. Gemmi A. Czopnik, and A. Jura, Phys. Rev. Lett. **86**, 4612 (2001).

[33] M.J. Besnus, J.P. Kappler, P. Lehmann, and A. Meyer, Solid State Commun. **55**, 779 (1985).

[34] J.P. Perdew and A. Zunger, Phys. Rev. B **23**, 5048 (1981).

[35] A. Swane and O. Gunnarson, Phys. Rev. Lett. **65**, 1148 (1990).

[36] A.B. Shick, A.I. Liechtenstein, and W.E. Pickett, Phys. Rev. B **60**, 10 763 (1999).

[37] A. Georges, G. Kotliar, W. Krauth, and M.J. Rozenberg, Rev. Mod. Phys. **68**, 13 (1996).